A comparison of implicit- and explicit-solvent simulations of self-assembly in block copolymer and solute systems

Cite as: J. Chem. Phys. **134**, 164902 (2011); https://doi.org/10.1063/1.3580293
Submitted: 07 December 2010 . Accepted: 07 March 2011 . Published Online: 28 April 2011

Justin R. Spaeth, Ioannis G. Kevrekidis, and Athanassios Z. Panagiotopoulos

A comparison of implicit- and explicit-solvent simulations of self-assembly in block copolymer and solute systems

Justin R. Spaeth,[1,a] Ioannis G. Kevrekidis,[1,2] and Athanassios Z. Panagiotopoulos[1,3]
[1]*Department of Chemical and Biological Engineering, Princeton University, Princeton, New Jersey 08544-5263, USA*
[2]*Program in Applied and Computational Mathematics, Princeton University, Princeton, New Jersey 08544-5263, USA*
[3]*Institute for the Science and Technology of Materials, Princeton University, Princeton, New Jersey 08544-5263,USA*

(Received 7 December 2010; accepted 7 March 2011; published online 28 April 2011)

We have developed explicit- and implicit-solvent models for the flash nanoprecipitation process, which involves rapid coprecipitation of block copolymers and solutes by changing solvent quality. The explicit-solvent model uses the dissipative particle dynamics (DPD) method and the implicit-solvent model uses the Brownian dynamics (BD) method. Each of the two models was parameterized to match key properties of the diblock copolymer (specifically, critical micelle concentration, diffusion coefficient, polystyrene melt density, and polyethylene glycol radius of gyration) and the hydrophobic solute (aqueous solubility, diffusion coefficient, and solid density). The models were simulated in the limit of instantaneous mixing of solvent with antisolvent. Despite the significant differences in the potentials employed in the implicit- and explicit-solvent models, the polymer-stabilized nanoparticles formed in both sets of simulations are similar in size and structure; however, the dynamic evolution of the two simulations is quite different. Nanoparticles in the BD simulations have diffusion coefficients that follow Rouse behavior ($D \propto M^{-1}$), whereas those in the DPD simulations have diffusion coefficients that are close to the values predicted by the Stokes–Einstein relation ($D \propto R^{-1}$). As the nanoparticles become larger, the discrepancy between diffusion coefficients grows. As a consequence, BD simulations produce increasingly slower aggregation dynamics with respect to real time and result in an unphysical evolution of the nanoparticle size distribution. Surface area per polymer of the stable explicit-solvent nanoparticles agrees well with experimental values, whereas the implicit-solvent nanoparticles are stable when the surface area per particle is roughly two to four times larger. We conclude that implicit-solvent models may produce questionable results when simulating nonequilibrium processes in which hydrodynamics play a critical role. © *2011 American Institute of Physics*. [doi:10.1063/1.3580293]

I. INTRODUCTION

Recently, there has been a rapidly growing interest in utilizing polymer-protected nanoparticles for drug delivery and medical imaging. Many useful drugs or imaging agents are insoluble in the bloodstream or are cleared by the kidneys before they can take effect.[1] One solution to this problem is to use amphiphilic block copolymer micelles as "containers" to carry such molecules.[2–21] The hydrophilic block forms a corona that sterically stabilizes the particles. In order to be useful, such particles must be sufficiently small (50–400 nm in diameter) and biocompatible.[4,11,20] One common choice for the hydrophilic block of the copolymer is polyethylene glycol (PEG), which has been shown to increase the circulation time of nanoparticles and facilitate the release of the drug molecules encapsulated within their cores.[2,4,10–13,15–17,19,21,22]

One of the most promising areas for nanoparticle-based drug delivery is in chemotherapy, where traditional delivery methods often result in widespread cell death throughout the body. Tuning the nanoparticle size can lead to preferential deposition in tumors, where the vasculature is different than in healthy tissue.[20,23] Additionally, polymers with ligands or receptor-specific peptide sequences bonded to the ends of the hydrophilic blocks can also be used to facilitate localized delivery.[7,11,19–21] Creating polymer-protected nanoparticles in the desired size range is nontrivial, however. In recent years, the "flash nanoprecipitation" technique was developed to produce nanoparticles by using rapid micromixing.[5,10–13,15,16,24] In this approach, block copolymer and hydrophobic solutes are first dissolved in an organic solvent in which both are soluble, then rapidly mixed with water at a high Reynolds number (>1600), creating a well-mixed solution in which the copolymer and solute are both highly supersaturated.[25] As the solutes aggregate to form clusters, the diblock copolymers begin to assemble on their surfaces, eventually halting their growth. Copolymer and solute concentrations, as well as the mixing stream velocities, can be adjusted to control the particle sizes. Even though such polymer-protected nanoparticles are now routinely synthesized, there is a lack of fundamental, molecular-level understanding of how the formation process proceeds. A detailed understanding of how and why some experimentally controllable parameters (such as hydrophilic

[a]Author to whom correspondence should be addressed. Electronic address: jspaeth@princeton.edu.

and hydrophobic block length and chemistry, compatibility between solute and polymer, and solute and polymer concentrations) affect the outcome of the experiments is still unavailable.

In the past few years, a number of computer simulation studies of systems containing block copolymers and nanoparticles have appeared. Some of these studies focused on systems in which no solvent is present at all (i.e., nanoparticle–polymer composites),[26–31] whereas others investigated the formation of polymer-protected nanoparticles in solvent.[12,32–35] Most of the latter were either carried out under conditions in which the polymer/solute/nanoparticle concentrations were substantially higher than those encountered in the flash nanoprecipitation process (ppm), or they did not employ a methodology that simulated the dynamic evolution of the system. For example, Chen *et al.*[33] used dissipative particle dynamics (DPD) to study a system containing solvent, diblock copolymers, and hydrophobic solutes, but the lowest solute and copolymer volume fractions studied were 10% and 5%, respectively. Likewise, the lowest solute and polymer concentrations employed by Huang *et al.*[32,35] were 6% and 2%, respectively. Chen *et al.* recently simulated the flash nanoprecipitation process at near-experimental concentrations using Brownian dynamics (BD) simulations of an implicit-solvent model, focusing on the effects of the solute–solute and solute–polymer interaction strengths on the nanoparticle size and polymer distribution on their surface.[12]

In this work, we develop a new explicit-solvent model and extend the implicit-solvent model of Chen *et al.*[12,36] for the flash nanoprecipitation process. Implicit-solvent models allow one to simulate larger systems for longer times than one can access with their explicit-solvent counterparts, especially when the vast majority of the system is comprised of solvent, as is the case here. We aim to explore whether there exist drawbacks associated with neglecting the solvent. Both models were parameterized based upon recent experiments of Kumar *et al.*,[13] in which flash nanoprecipitation was used to produce polymer-stabilized nanoparticles filled with the antifungal drug itraconazole and stabilized by the diblock copolymer polystyrene-*b*-polyethylene glycol (PS_{10}-*b*-PEG_{68}, PS block molecular weight 1000 and PEG block molecular weight 3000). In the remainder of this paper, the term *solute* refers to a hydrophobic entity that enters the nanoparticle core during the flash nanoprecipitation process, and the term *diblock* refers to a diblock copolymer that acts as the stabilizer during the process.

Three major challenges arise when attempting to simulate the flash nanoprecipitation process at the experimental conditions. First, the mixing time has been estimated to be in the range of milliseconds.[5,10–12,16] Second, the concentrations of the solute and diblock are, respectively, ∼30 and ∼5.3 molecules per million solvent molecules (after mixing).[13] Third, a typical nanoparticle formed in the process has a diameter around 100 nm or greater and contains hundreds of thousands of solute molecules.[10–13] Hence, a simulation containing enough material to form even a single 100 nm particle must employ a cubic domain of ∼500 nm in each direction and contain hundreds of thousands of solute and diblock molecules and billions of solvent molecules. In addition to being nearly computationally intractable due to its size, simulating such a large system for milliseconds is clearly impractical.

In order to address these difficulties, we make simplifications to render the problem computationally tractable. First, we use polymer and solute concentrations (and supersaturation ratios) roughly ten times higher than those in the experimental system; consequently, there is an upper bound on the size of the nanoparticles that can form in our simulations, dictated by the total number of polymers and solutes in the system. Also, our simulations are performed with "infinitely fast mixing"—the diblocks and solutes are randomly mixed prior to being exposed to the very poor solvent conditions which cause them to aggregate. The mixing time has a significant impact on the kinetics of the self-assembly process[5,10–12] but studying its effects is beyond the scope of this work. We aim to show that, while the structure of the nanoparticles formed in the implicit- and explicit-solvent simulations are quite similar, the dynamical evolution of the system is quite different between the two.

The structure of this paper is as follows. In Sec. II, we discuss the parameterization of each of the two models and the methods used to simulate them. In Sec. III, we present and analyze the results of the simulations, beginning with the dynamic evolution. Next, we compare the sizes and structures of the nanoparticles formed. Then, we compare nanoparticle diffusion coefficients to the theoretical values given by the Stokes–Einstein relationship. We also compare the stability of implicit-solvent and explicit-solvent nanoparticles, including the average surface area occupied by a diblock in both models. We conclude with a summary of our results and their implications on future attempts to simulate such dynamically evolving nonequilibrium systems.

II. MODELS AND METHODS

A. Implicit-solvent model

1. Characteristic scales

The implicit-solvent model for PS_{10}-*b*-PEG_{68} of Chen *et al.*[36] serves as the foundation for our implicit-solvent model. The characteristic length, mass, and energy are L_{BD} = 1.82 nm, m_{BD} = 375 Da, and ε_{BD}/k_B = 372.5 K, where k_B is the Boltzmann constant. The characteristic length was determined in Ref. 36 by matching the prefactor of the radius of gyration scaling law for the PEG model employed therein, and the characteristic mass was set equal to the mass of a coarse-grained PEG bead. The simulations in Ref. 36 were run at a dimensionless temperature of $T^* = k_BT/\varepsilon_{BD} = 0.8$, representing a real temperature of $T = 298$ K. The intrinsic time scale, which results from nondimensionalization of the equations of motion, is given by the following relation:

$$\tau_{\text{intrinsic},BD} = L_{BD}\sqrt{\frac{m_{BD}}{\varepsilon_{BD}}}, \tag{1}$$

and is equal to 20 ps.

2. Interaction parameters

In this section, all equations and simulation parameters are given in real units, with the energies given as multiples of ε_{BD}. In the remainder of the paper, we will use the subscript w for the solvent, s for the solute, e for PEG, and p for PS. The diblock copolymer description within the implicit-solvent model is identical to that developed by Chen *et al.*[36] The PEG portion of the diblock is represented by eight solvophilic beads of $m_e = 375$ Da and diameter $\sigma_{ee} = 1.82$ nm that interact with one another via a Gaussian repulsion potential of the form

$$U(r) = \varepsilon \left[\exp\left(\frac{-6r^2}{\sigma^2}\right) + \exp\left(\frac{-6r_{\text{cut}}^2}{\sigma^2}\right)\right], \tag{2}$$

where ε is the energy parameter, r is the distance between particles, and r_{cut} is the cutoff distance. The PS portion of the diblock is represented by five smaller, lighter beads ($m_p = 200$ Da and $\sigma_{pp} = 0.73$ nm) that interact with one another via a cut-and-shifted Lennard-Jones (LJ) 9-6 potential:

$$U(r) = \frac{27}{4}\varepsilon \left[\left(\frac{\sigma}{r}\right)^9 - \left(\frac{\sigma}{r}\right)^6 - \left(\frac{\sigma}{r_{\text{cut}}}\right)^9 + \left(\frac{\sigma}{r_{\text{cut}}}\right)^6 \right], \tag{3}$$

where σ is the LJ size parameter. The 13 beads comprising the diblock are connected via harmonic bonds between neighboring beads:

$$F_{\text{bond}} = k\left(r_{ij} - r_0\right), \tag{4}$$

with $k = 15.5$ N/m and $r_0 = \sigma_{ij}$, where r_{ij} is the distance between the neighboring bonded beads and σ_{ij} is the LJ size parameter for the two beads involved in the bond. The PEG and PS beads also interact with one another via a cut-and-shifted LJ 9-6 potential, except for the two beads involved in a bond, which interact only via the bond potential. The PEG–PEG interaction was parameterized to give the proper scaling of the radius of gyration and second virial coefficient with chain length for PEG chains in water, and the PS–PS interaction and PEG–PS interactions were parameterized to match the critical micelle concentration (CMC) and aggregation number of the diblock in water at room temperature, as described in Ref. 36.

In Chen *et al.*,[12] generic single-bead hydrophobic solutes were introduced in BD simulations in order to simulate the flash nanoprecipitation process, but the interactions were not parameterized to specific real systems. In the present work, we also use a single-bead description of the solute, but we choose the size, mass, and solute–solute interaction parameters to match the molecular density, molecular mass, and solubility of itraconazole in water. Itraconazole has a molecular mass of 708 Da,[13] so we set $m_s = 708$. For the interactions between solute beads we used a LJ 12-6 potential:

$$U(r) = 4\varepsilon \left[\left(\frac{\sigma}{r}\right)^{12} - \left(\frac{\sigma}{r}\right)^6 \right]. \tag{5}$$

Agrawal and Kofke[37] determined coexisting vapor and solid densities for this system below the triple point temperature. The solubility of itraconazole in a 4.7% tetrahydrofuran solution (final solvent composition in flash nanoprecipitation experiments) is 1.18×10^{-4} mol/m^3 and the solid density is 1.38 g/ml at 278 K.[13] In order to obtain such a low vapor phase density for the LJ 12-6 fluid, the data of Ref. 37 were extrapolated to lower temperatures. At a reduced temperature $T^* = 0.32$, setting $\sigma = 0.96$ nm, the extrapolated solid and vapor densities are 1.40 g/ml and 1.05×10^{-4} mol/m^3, respectively, in close agreement with the experimental values for itraconazole. Hence, we used $\varepsilon_{ss} = 2.5\varepsilon_{BD}$ and $\sigma_{ss} = 0.96$ nm for the LJ 12-6 potential between solute beads.

Following Ref. 36, the interaction between the solute and PEG beads is a purely repulsive cut-and-shifted LJ 9-6 potential, and the interaction between the solute and PS beads is a cut-and-shifted LJ 9-6 potential with a longer cutoff that includes the attractive tail. The LJ size parameter σ for these interactions was taken as the arithmetic mean of the corresponding pure-component size parameters. The LJ energy parameter for the solute–PEG interaction was taken to be $\varepsilon_{se} = \varepsilon_{BD}$, as in the work by Chen *et al.*[12] Finally, for the LJ energy parameter for the solute–PS interaction, we investigated two different values, $\varepsilon_{sp} = 1.3\ \varepsilon_{BD}$ and $\varepsilon_{sp} = 2.5\ \varepsilon_{BD}$, chosen qualitatively to represent an "unfavorable" and "favorable" interaction, respectively. Table I summarizes the energy, size, and cutoff parameters for the interactions in the implicit-solvent model.

3. Simulation details

BD simulations were carried out using the LAMMPS simulation package.[38] We initialized the simulation by randomly placing 1200 solute beads and 215 diblocks in a $50 \times 50 \times 50$ nm box and then using Monte Carlo moves to eliminate any overlaps. The concentrations of the solute and diblock that we used (9.6×10^{-3} and 1.72×10^{-3} molecules/nm^3, respectively) are both approximately ten times larger than the experimental concentrations in the experiments of Kumar *et al.*[13] The force on particle i is governed by the Langevin equation

$$m_i \boldsymbol{a}_i = \sum_{j \neq i} \mathbf{F}_{ij}^C - m_i \gamma \boldsymbol{v}_i + \sqrt{2 m_i \gamma k_B T \Delta t_{BD}}\,\theta_i, \tag{6}$$

where m_i is the particle's mass, $\mathbf{a}_i$ is the acceleration on the particle, $\mathbf{F}_{ij}^C$ is the conservative pairwise force on particle i due to particle j, γ is the friction coefficient, $\mathbf{v}_i$ is the particle's velocity, Δt_{BD} is the time step, and θ_i is a Gaussian random number with unit variance that is delta-correlated in time:

$$\langle \theta_i(t) \rangle = 0, \tag{7}$$

$$\left\langle \theta_i(t)\, \theta_i\left(t'\right) \right\rangle = \delta\left(t - t'\right). \tag{8}$$

The equations of motion were integrated using the velocity-Verlet algorithm with a time step of $\Delta t_{BD} = 60$ fs and a friction coefficient of $\gamma = 50$ ns^{-1} at fixed temperature of $T = 298$ K.

B. Explicit-solvent model

For the explicit-solvent model, we used the DPD method.[39,40] DPD employs soft, purely repulsive forces between particles, which are also subject to a random, impulsive force and a frictional, dissipative force. These forces together

TABLE I. Pairwise interaction parameters for the implicit-solvent model studied with BD simulations. Energies are given as multiples of ε_{BD}, where $\varepsilon_{BD}/k_B = 372.5$ K.

Pair type	Potential	$\varepsilon/\varepsilon_{\mathrm{BD}}$	σ (nm)	Cutoff distance r_{cut} (nm)
Solute–solute (*ss*)	LJ 12-6	2.5	0.960	$2(3/2)^{1/3}\sigma_{ss}$
Solute–PS (*sp*)	LJ 9-6	2.5 (favorable) 1.3 (unfavorable)	0.844	$2(3/2)^{1/3}\sigma_{sp}$
Solute–PEG (*se*)	LJ 9-6	1.0	1.390	$(3/2)^{1/3}\sigma_{se}$
PS–PS (*pp*)	LJ 9-6	1.3	0.728	$2(3/2)^{1/3}\sigma_{pp}$
PS–PEG (*pe*)	LJ 9-6	0.01	1.274	$(3/2)^{1/3}\sigma_{pe}$
PEG–PEG (*ee*)	Gaussian	1.0	1.820	$1.2\sigma_{ee}$

act as a thermostat and cause the system to rigorously sample the canonical (NVT) ensemble.[41] The system evolves according to Newton's equations of motion, with the force on each particle being given by the sum of the repulsive conservative force $\mathbf{F}^C$, the impulsive force $\mathbf{F}^R$, and the dissipative force $\mathbf{F}^D$:

$$\mathbf{f}_i = \sum_{j \neq i} \left(\mathbf{F}_{ij}^C + \mathbf{F}_{ij}^R + \mathbf{F}_{ij}^D \right), \tag{9}$$

$$\mathbf{F}_{ij}^C = a_{ij} \left(1 - \frac{r_{ij}}{r_c} \right) \hat{\mathbf{r}}_{ij}, \tag{10}$$

$$\mathbf{F}_{ij}^R = \frac{\sigma_{ij}\theta_{ij}}{\sqrt{\Delta t_{DPD}}} \left(1 - \frac{r_{ij}}{r_c} \right) \hat{\mathbf{r}}_{ij}, \tag{11}$$

$$\mathbf{F}_{ij}^D = -\gamma_{ij} \left(1 - \frac{r_{ij}}{r_c} \right)^2 \left(\hat{\mathbf{r}}_{ij} \cdot \mathbf{v}_{ij} \right) \hat{\mathbf{r}}_{ij}. \tag{12}$$

In the above equations, a_{ij} is the maximum repulsion between particles i and j, r_{ij} is the distance between particles i and j, $\hat{\mathbf{r}}_{ij} = \left(\mathbf{r}_i - \mathbf{r}_j\right)/r_{ij}$ is the unit vector pointing from particle j to particle i, $\mathbf{v}_{ij} = (\mathbf{v}_i - \mathbf{v}_j)$ is the relative velocity of particle i to particle j, θ_{ij} is a Gaussian-distributed random number with zero mean and unit variance, Δt_{DPD} is the size of the time step used in integrating the equations of motion, and σ_{ij} and γ_{ij} are multiplicative constants (also referred to as the noise parameter and friction coefficient, respectively). All forces vanish beyond the cutoff radius, r_c. The fluctuation–dissipation relation[41] requires that

$$\sigma_{ij}^2 = 2\gamma_{ij} k_B T. \tag{13}$$

For further details on the DPD method, we refer the reader to the original paper of Groot and Warren.[40]

1. Characteristic scales

The characteristic length, mass, and energy for the explicit-solvent model are $L_{DPD} = 1$ nm, $m_{DPD} = 200$ Da, and $\varepsilon_{DPD}/k_B = 298$ K. The characteristic length was chosen *a priori*, and the characteristic mass is equal to the mass of a coarse-grained PS bead, which represents two real PS monomers. The intrinsic time scale for the DPD simulations, calculated as in (1), is $\tau_{\mathrm{intrinsic},DPD} = 9$ ps.

2. Coarse-grained mapping

We set the particle mass and DPD cutoff radius equal to one another for each of the four types of particles in the system, as is typical in the literature for DPD simulations ($m_i = 200$ Da and $r_c = 1$ nm). We used a solvent bead density $\rho = 3.0$ nm^{-3} (reduced density equal to 3) and let each DPD solvent bead represents 11 water molecules. This gives a solvent mass density of 0.988 g/cm^3, roughly matching the mass density of liquid water (1 g/cm^3). Kumar *et al.*[13] determined the solid density of itraconazole to be 5.1×10^{-4} m^3/mol, or ~0.85 nm^3/molecule. We represent the solute (itraconazole) as three DPD beads bound together in a chain by harmonic bonds with equilibrium length $r_o = 0.8$ nm and spring constant $k = 0.25$ N/m. When these DPD trimers collapse in the presence of bad solvent and aggregate in the core of the nanoparticle, we expect that they will on average occupy 1 nm^3 per molecule, roughly matching the solid density of itraconazole. The diblock being modeled was PS_{10}-*b*-PEG_{68}, which contains ten PS monomers and 68 PEG monomers. For the PS beads in the diblock, we matched the experimental melt density of 1.05 g/cm^3, or approximately six monomers per nm^3, by mapping two PS monomers onto each coarse-grained PS bead, giving a PS block length of five for the model diblock. Finally, for the PEG portion of the diblock, we matched the radius of gyration (R_g) of PEG_{68} in water to experimental values. We graphically extrapolated the experimental results of Kawaguchi *et al.*[42] to obtain a value of $\langle R_g \rangle \approx 1.87$ nm. With the repulsion parameter between the solvent and PEG beads used in this work ($a_{we} = 25\varepsilon_{DPD}$, which we will discuss shortly), a DPD chain containing 20 beads gave $\langle R_g \rangle = 1.83$ nm, in good agreement with the experimental value previously mentioned; thus, we represented the 68 PEG monomers in the real diblock by 20 coarse-grained DPD PEG beads. As with the solute molecule, beads in the diblock are connected via harmonic bonds with $r_0 = 0.8$ nm and $k = 0.25$ N/m. In contrast to the implicit-solvent model, the repulsive DPD potential is not switched off for neighboring beads in a chain that are connected via a bond.

3. Interaction parameter determination

We set all four like-particle repulsion parameters equal to $a_{ii} = 25\varepsilon_{DPD}$, as is common when using DPD. The repulsion parameter between solvent and PEG beads was also $a_{we} = 25\varepsilon_{DPD}$. We performed a series of simulations for various chain lengths from 3 to 30 and found that this solvent–PEG model gives a chain-length scaling exponent of 1.09 for the square of the radius of gyration, in close agreement

with the experiments of Kawaguchi *et al.*,[42] who obtained a value of 1.1.

Once the chain architecture and other parameters are set, interactions between the hydrophobic PS beads and the solvent determine the CMC of the diblock. The CMC of PS_{10}-*b*-PEG_{68} is $\sim 1 \times 10^{-3}$ wt. % in water at room temperature.[43] This is too dilute to be directly simulated, even with the coarse-grained solvent we are using. Instead of directly calculating the CMC of our model diblock, heretofore referred to as $H_{20}T_5$ (20 hydrophilic PEG beads and five hydrophobic PS beads), we instead computed the CMC of $H_{20}T_2$, $H_{20}T_3$, and $H_{20}T_4$ and extrapolated the results to $H_{20}T_5$, repeating the procedure for a few different values of the PS–solvent repulsion parameter. In each case, we fixed the repulsion parameter between PS and PEG beads at $a_{pe} = 40\ \varepsilon_{DPD}$, the value used by Sheng *et al*. in a recent DPD study of diblock copolymer micellization.[44] For each chain architecture and PS–solvent repulsion parameter, we ran a long (2×10^6 time steps) DPD simulation at a diblock concentration above the CMC. Once the system equilibrated, we calculated an aggregate size distribution, averaged over 10^6 time steps, and used it to determine the CMC. We determined the location of the minimum in the aggregate size distribution and counted all diblocks in aggregates smaller than that size toward the CMC. We found that a solvent–PS repulsion parameter of $a_{wp} = 54\ \varepsilon_{DPD}$ gave CMCs (in wt. %) for $H_{20}T_2$, $H_{20}T_3$, and $H_{20}T_4$ of 2.7±0.7, 0.13±0.02, and 0.012±0.003, with the averages and standard deviations calculated by breaking the equilibration period into ten independent blocks. Theoretical[45] and experimental[46] studies have shown that the logarithm of the CMC of a diblock copolymer decreases linearly with hydrophobic block length. The extrapolated CMC for $H_{20}T_5$ based on the above values is $(8\pm3) \times 10^{-4}$ wt. %, in good agreement with the experimental CMC of PS_{10}-*b*-PEG_{68}.

In Ref. 36 both the CMC and aggregation number were matched to experimental values by adjusting the PS–PS and PS–PEG interactions. In the case of our explicit-solvent model, we were unable to match both quantities. Given that a repulsion parameter between unlike beads of 25 ε_{DPD} produces perfect mixing (since the like-particle repulsion parameters are $a_{ii} = 25\ \varepsilon_{DPD}$) and that the solvent–PS repulsion parameter is $a_{wp} = 54\ \varepsilon_{DPD}$, the PS–PEG repulsion parameter should fall somewhere between these values. Repulsion parameters of $a_{pe} = 30\ \varepsilon_{DPD}$ and $a_{pe} = 40\ \varepsilon_{DPD}$ resulted in a nearly identical weight-averaged aggregation number of 22, whereas the experimental value reported by Bronstein *et al.*[47] is 41. Hence, for the remainder of the simulations discussed in this work, we held the PS–PEG repulsion parameter fixed at $a_{pe} = 40\ \varepsilon_{DPD}$.

The remaining repulsion parameters involve the solute, which we model as a trimer. The repulsion parameter between the solute beads in the trimer and the solvent beads was determined on the basis of matching the experimental solubility of itraconazole, 1.18×10^{-4} mol/m^3. Accounting for the coarse-graining of the solvent and the volume of the solute, this is equal to a solute volume fraction of $\sim 7 \times 10^{-8}$. Phase diagrams for DPD chains in monomer solvent with a dimensionless bead density of 3 are available.[48,49] By extrapolating to trimers in monomeric solvent, we find that the solute volume fraction ($\sim 7 \times 10^{-8}$) is matched when the repulsion parameter between the solute beads and solvent beads is $a_{ws} \approx 68\ \varepsilon_{DPD}$.

TABLE II. Repulsion parameters used in the explicit-solvent DPD simulations, in units of ε_{DPD}, where $\varepsilon_{DPD}/k_B = 298$ K.

	Solvent	Solute	PS	PEG
Solvent	25	68	54	25
Solute	68	25	25 (favorable) 35 (unfavorable)	35 (favorable) 55 (unfavorable)
PS	54	25 (favorable) 35 (unfavorable)	25	40
PEG	25	35 (favorable) 55 (unfavorable)	40	25

Finally, for the two repulsion parameters defining the interaction of the solute with the diblock (a_{sp} and a_{se}), there are no suitable itraconazole–diblock data that can be used to carry out a parameterization. As with the implicit-solvent model, we investigated two different sets of values for these parameters—one set for favorable solute–diblock interactions, and a second set for unfavorable interactions. For the favorable interactions, we chose the solute–PS repulsion parameter to be $a_{sp} = 25\ \varepsilon_{DPD}$ and the solute–PEG repulsion parameter to be $a_{se} = 35\varepsilon_{DPD}$. Here, $a_{sp} = 25\varepsilon_{DPD}$ represents the case where the solute and PS beads interact and mix as well with one another as they do with beads of their own type, and $a_{se} = 35\varepsilon_{DPD}$ represents a slightly unfavorable interaction, but not nearly as unfavorable as that between the solute and solvent. For the unfavorable case, we chose the solute–PS repulsion parameter to be $a_{sp} = 35\varepsilon_{DPD}$ and the solute–PEG repulsion parameter to be $a_{se} = 55\varepsilon_{DPD}$. Table II summarizes the repulsion parameters used in the explicit-solvent DPD simulations.

4. Friction coefficients

For the explicit-solvent model, we attempted to match the ratio of the solute and diblock diffusion coefficients. Since no experimental diffusion coefficient is available for itraconazole, we estimated it by using the Stokes–Einstein relationship

$$D = \frac{k_B T}{6\pi \mu r}, \tag{14}$$

using the viscosity of water at 298 K. Taking the solute radius to be $r = 0.62$ nm (the radius of a sphere with a volume of 1 nm^3, the solute volume), we estimated a solute diffusion coefficient of 3.93×10^{-6} cm^2/s. The experimental diffusion coefficient of the diblock reported by Bronstein *et al.*[47] is 1.26×10^{-6} cm^2/s, 3.12 times smaller than the estimated solute diffusion coefficient. The DPD friction parameters provide "knobs" which one can tune to make adjustments to the solute and diblock diffusion coefficients. Following other DPD simulations in the literature,[32,33,35,40,50,51] we first chose the friction coefficients for all interactions to be $\gamma_{ij} = 500$ ns^{-1} (4.5 in

dimensionless units). Preliminary simulations indicated the ratio of the solute to diblock diffusion coefficients to be too low. Decreasing the solvent–solute friction parameter to $\gamma_{ws} = 111$ ns^{-1} (1.0 in dimensionless units) and increasing the solvent–PEG and solvent–PS friction parameters (γ_{we} and γ_{wp}) to 2000 ns^{-1} (18.0 in dimensionless units) produced the desired result, a solute-to-diblock diffusion coefficient ratio of around 3.1.

5. Simulation details

DPD simulations of the explicit-solvent model were carried out using the LAMMPS simulation package.[38] We initialized the simulation by randomly placing 366 025 solvent beads, 1200 solute molecules, and 215 diblocks in a 50 × 50 × 50 nm box (same system as in the implicit-solvent simulations). The simulation was started directly from the random initial configuration—no energy minimization is required to eliminate particle overlaps, due to the softness of the DPD potential. The equations of motion for the system were integrated with a time step of $\Delta t = 0.36$ ps.

C. Nanoparticle identification

In order to analyze nanoparticles during the self-assembly process, a cluster list was constructed from each snapshot of particle positions by looping over all molecules (solutes and diblocks) and determining, for each molecule, which other molecules were in the same cluster. For the diblocks, only the PS portion of the chain was considered during cluster determination. Two molecules were considered to be in the same cluster if any of the beads in one molecule (PS beads only for the diblocks) were within a cutoff distance of any of the beads in the other molecule. For the implicit-solvent model, the cluster cutoff distance for a pair of beads of type i and j was taken as $\sqrt{2}\sigma_{ij}$ (see Table I). For the explicit-solvent model, in which all particle sizes and potential cutoff radii are the same, the cluster cutoff distance was taken to be 0.85 nm, roughly the distance at which the first maximum appears in the pair correlation function for a monomeric DPD fluid with $a_{ii} = 25\varepsilon_{DPD}$ and dimensionless bead density of 3.[48,52]

D. Rescaling of time

Implicit-solvent BD simulations and explicit-solvent DPD simulations are both known to produce accelerated dynamics (with respect to full atomistic MD) when the intrinsic time scale is used as a measure of time. A common and more meaningful way of interpreting the dynamics of coarse-grained simulations is to rescale time so that some fundamental dynamic property of the system (in our case, the center-of-mass diffusion coefficient of a single diblock at infinite dilution) is matched. The idea of obtaining the time scale through the matching of diffusion coefficients has been employed by Groot[51,53,54] and was recently discussed by Füchslin *et al.*[55] For the implicit-solvent model, we simulated a single diblock chain and determined that a characteristic time $\tau_{BD} = 2.5$ ns resulted in a diffusion coefficient of 1.26×10^{-6} cm^2/s, the value experimentally determined in Ref. 47. This new BD time scale is 125 times greater than the intrinsic BD time scale of 20 ps, which is a result of coarse-graining. For the explicit-solvent model, we simulated a single diblock in solvent and determined that a characteristic time $\tau_{DPD} = 250$ ps was needed to match the diffusion coefficient to the experimental value. This new DPD time scale is roughly 28 times greater than the intrinsic DPD time scale of 9 ps, due to the soft nature of the DPD potential. All results presented in the following sections use the rescaled measures of time. However, we would like to point out that for any nondimensionalization of simulation input parameters involving time, it is appropriate to use the intrinsic time scale, which is derived from the equations of motion, rather than from an *a posteriori* analysis of simulation results.

III. RESULTS AND DISCUSSION

A. Dynamics of aggregation

Figure 1 shows the number of nanoparticles, weight-averaged number of solutes per nanoparticle, and weight-averaged number of diblocks per nanoparticle as a function of time for the four different cases (favorable and unfavorable solute–diblock interaction, each for the implicit and the explicit model). The weight-averaged number of molecules per nanoparticle is defined as

$$\langle N \rangle_w = \sum_{\text{clusters},i} \frac{N_i^2}{N_{\text{clustered}}}, \tag{15}$$

where N_i denotes the number of molecules in cluster i, and $N_{\text{clustered}}$ denotes the total number of molecules contained in aggregates. Only nanoparticles containing at least two solute molecules (but any number of diblocks) are considered in the calculation. Particle positions were analyzed every 10 ns for the DPD simulations and every 37.5 ns for the BD simulations. The visual "steps" in the graphs are the result of fusion events between aggregates. It is clear that self-assembly in the BD simulations takes place more slowly than in the DPD simulations. As will be discussed in Sec. III C, nanoparticle diffusion coefficients in the BD simulations are smaller than for the DPD simulations. This leads to fewer nanoparticle collisions in a given amount of time and slower growth. Another possible cause for the slower growth may be that collisions between two nanoparticles in the BD simulations are less likely to lead to fusion.

A reasonable starting point for a theoretical description of the aggregation dynamics of this system would be a diffusion-limited Smoluchowski approach, namely, the model investigated by Marrink *et al.*[56,57] We numerically solved the governing equations up to a maximum cluster size of 1200 solutes (the maximum number of solutes in our system), substituting the Stokes–Einstein expression for the diffusion coefficient into the rate constant expression. In Fig. 2, we show the distribution of solutes in clusters of different sizes after 30 and 70 ns for the implicit- and explicit-solvent simulations with favorable solute–polymer interactions. Rescaling the time by a factor of 0.75 in the theoretical model predictions produces

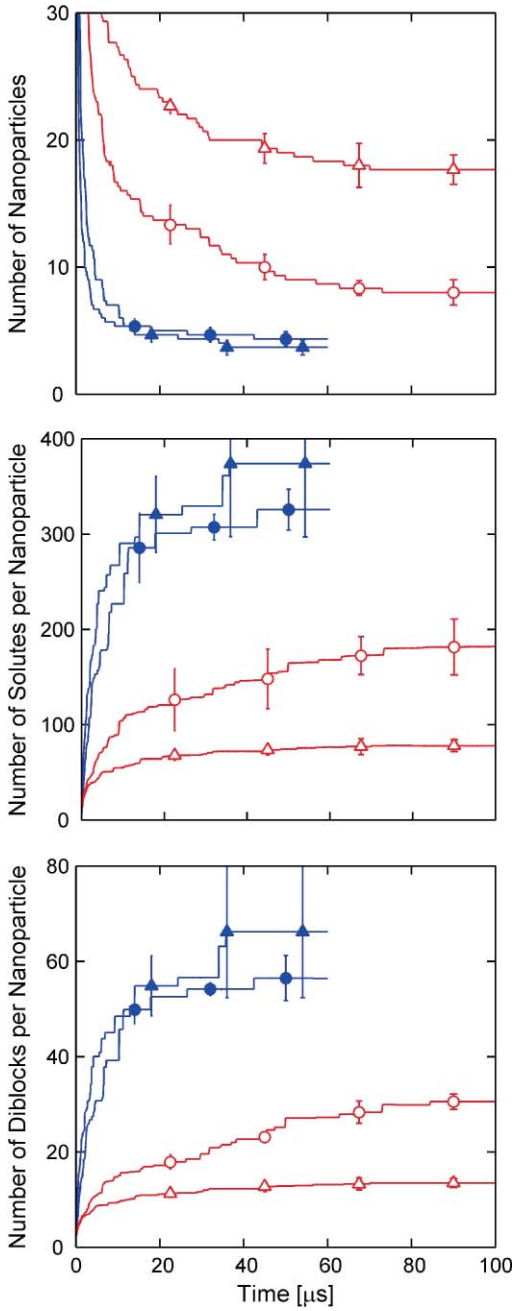

FIG. 1. Number of nanoparticles, weight-averaged number of solute molecules per nanoparticle, and weight-averaged number of diblock molecules per nanoparticle vs time. Results shown are an average of three randomly initialized simulations, with the error bars showing standard deviations at a few points during the simulation. Solid symbols are for DPD simulations and open symbols are for BD simulations. Triangles are for favorable solute–PS interaction and circles for unfavorable solute–PS interaction.

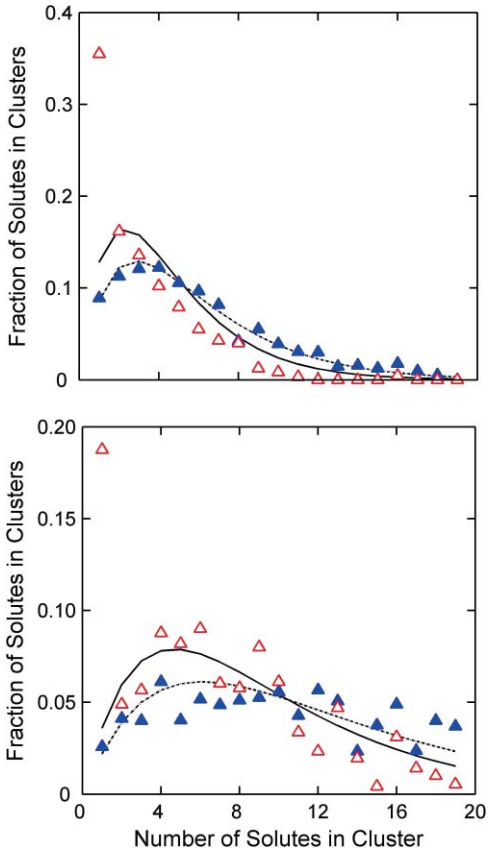

FIG. 2. Distribution of solutes in clusters of different sizes after 30 ns (top) and 70 ns (bottom). Clusters containing 20 or more solutes were included in the calculation but are not shown in this figure. The solid line represents a theoretical prediction based upon a diffusion-limited Smoluchowski approach (Ref. 56). The dashed line represents the same theoretical prediction, but with the time rescaled by a factor of 0.75. Symbols are as in Fig. 1.

good agreement with the explicit-solvent simulations. However, no such rescaling of time produces agreement with the implicit-solvent simulation results. Due to the finite size of our system, the cluster size distribution deteriorates as time progresses. It is worth noting that, as polymers attach to the solute clusters, collisions between clusters may not always result in fusion, which violates the assumptions built into the theory. Better agreement with theoretical predictions might be found by simulating larger systems containing only solutes, but such investigations fall outside our current focus.

In Fig. 3, we have plotted the weight-averaged number of diblocks per nanoparticle versus the weight-averaged number of solutes per nanoparticle at a few different instances in time during the simulations. Although the simulations may evolve at different rates in real time, we see that the number of diblocks per nanoparticle appears to be slaved to the number of solutes per nanoparticle. In all four simulations, the ratio of the weight-averaged number of diblocks and solutes per nanoparticle is essentially equal to the overall ratio of their concentrations.

As nanoparticles begin to fuse, the surface area to volume ratio goes down, but the number of solutes and diblocks in the simulation are fixed. In all four sets of simulations, after a short initial period, there are no solutes or diblocks that are not part of an aggregate. When two nanoparticles collide, the solute-filled cores fuse together, and the diblocks that were on the surfaces of the individual particles rearrange on the surface of the new, larger aggregate. Consequently, as the self-assembly process proceeds, the number of diblocks per unit surface area increases, and the nanoparticles become more stable.

There is a substantial difference in the stability of the same size nanoparticles in the BD simulations and DPD

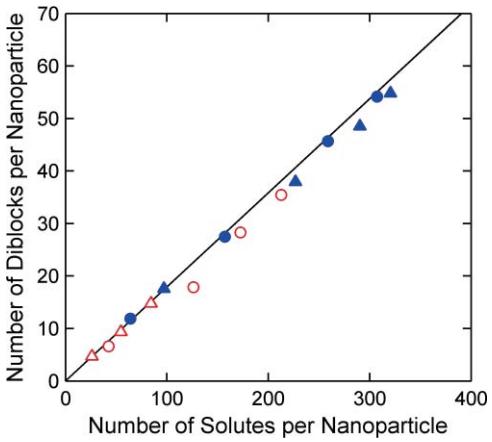

FIG. 3. Number of diblocks per nanoparticle vs number of solutes per nanoparticle (both weight-averaged) at various points in time during in the simulations. The solid line represents the ratio between the total number of polymers and solutes present in the simulations. Symbols are as in Fig. 1.

simulations. This is most clearly illustrated by comparing the simulations with favorable solute–PS interactions in Fig. 1. The implicit-solvent nanoparticles stop fusing when the weight-averaged number of solutes and diblocks per nanoparticle are ∼85 and ∼15, respectively, whereas this does not occur in the explicit-solvent simulations until there are ∼375 solutes and ∼66 diblocks per nanoparticle.

B. Nanoparticle structure and size

Figure 4 shows snapshots from the end of a DPD simulation (top) and a BD simulation (bottom) for the case of favorable solute–PS interactions. The DPD nanoparticles are clearly larger than the BD ones, because DPD particles continued to fuse and grow past the limit at which the BD particles became stable. However, in both cases, we see that the PS (red beads) is distributed on the surface evenly and the PEG (transparent gray beads) is well spread out around the cores of the nanoparticles. In contrast, Fig. 5 shows snapshots from the end of a DPD simulation (top) and a BD simulation (bottom) for the case of unfavorable solute–PS interactions. In both images, clustering of the PS blocks on the nanoparticle surfaces is readily apparent, leaving larger regions of the solute core (blue beads) exposed to the solvent without PEG stabilization. A movie of a simulation corresponding to each snapshot in Figs. 4 and 5 can be found in the supplementary material.[58]

In Figs. 6–10, each data point corresponds to a different nanoparticle, with data averaged over a long time period (typically longer than 10 μs) after it has been confirmed that the nanoparticle is stable and no longer growing. In Fig. 6, we plot the radius of gyration of all solute beads versus the number of solute molecules; particles formed in both the BD and DPD simulations share the same "core" size as a function of the number of solute molecules those cores contain. In both cases, the simulations with the favorable solute–PS interaction give a slightly larger radius of gyration for the solute core, due to slight penetration of PS beads into the core, as shown in Fig. 7. Recall that in the implicit-solvent model, a solute molecule is represented by a single bead, whereas in the explicit-solvent model it is represented by a trimer. This confirms that our *a priori* attempt at matching the solute solid density between both models was successful.

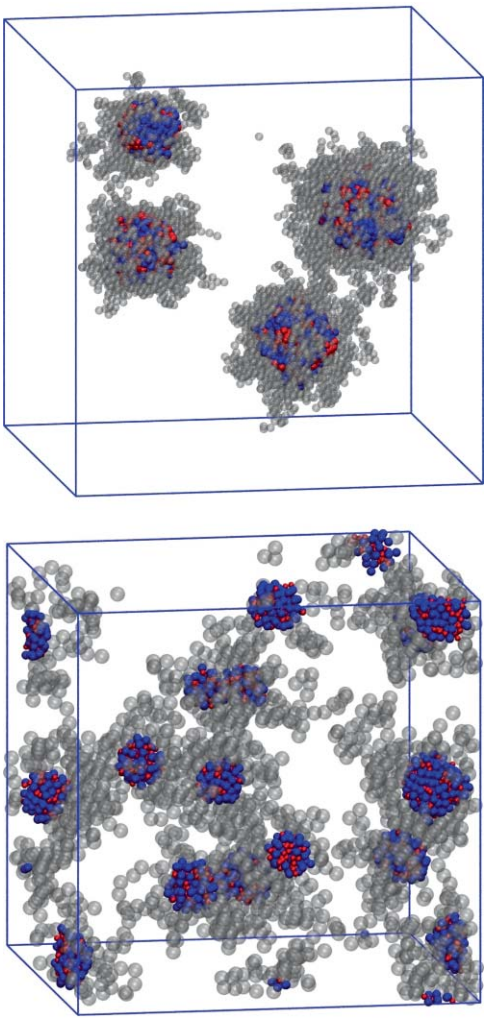

FIG. 4. Snapshot of nanoparticles formed in a DPD simulation (top) and BD simulation (bottom) with favorable solute–PS interactions. The solute beads are shown in blue, PS beads in red, and PEG beads as transparent gray. Note the uniform coverage of PS beads on the nanoparticle surface and the uniform distribution of PEG chains around the outside of the nanoparticles. Movie files of a DPD simulation (movie 1) and a BD simulation (movie 2) are available (Ref. 58).

In Fig. 7 we show the extent to which PS beads penetrate into the nanoparticle core. The maximum solute radius is defined as the maximum distance between any solute bead and the nanoparticle's center of mass, and the PS to center-of-mass distance is an average over all PS beads in the nanoparticle. The solid black line of unit slope represents the case in which PS beads sit (on average) directly on the particle surface, as is the case for the BD model simulations with unfavorable solute–PS interactions. Similar behavior is seen for the DPD simulations with unfavorable solute–PS interactions, but, in this case, the beads do penetrate the surface slightly. The primary reason for the minor difference lies in the nature of the potentials employed. The truncated LJ potential used in the implicit-solvent model is steeply repulsive at short distances and does not allow the PS beads to go past the

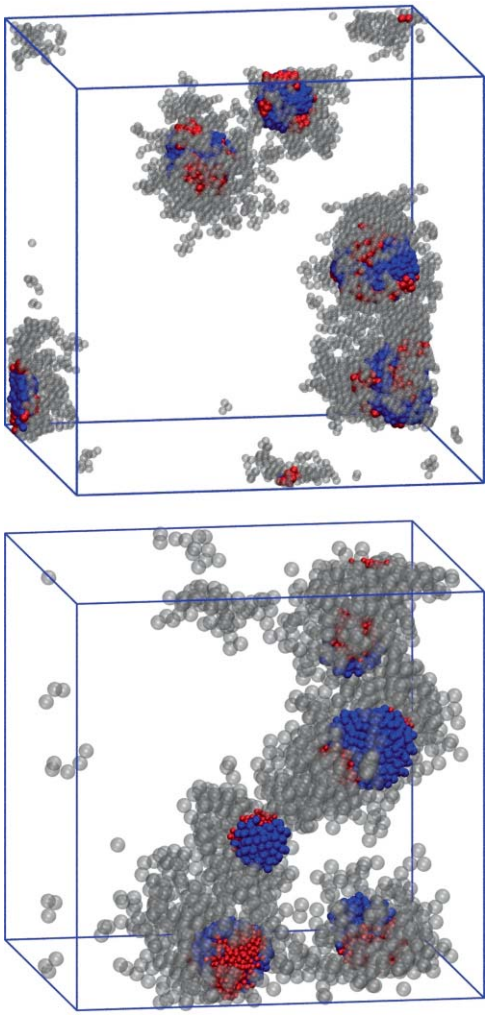

FIG. 5. Snapshot of nanoparticles formed in a DPD simulation (top) and BD simulation (bottom) with unfavorable solute–PS interactions. The color scheme for the beads is the same as in Fig. 4. Note the clustering of PS beads on the nanoparticle surface, which leaves large areas of the core exposed. Movie files of a DPD simulation (movie 3) and a BD simulation (movie 4) are available (Ref. 58).

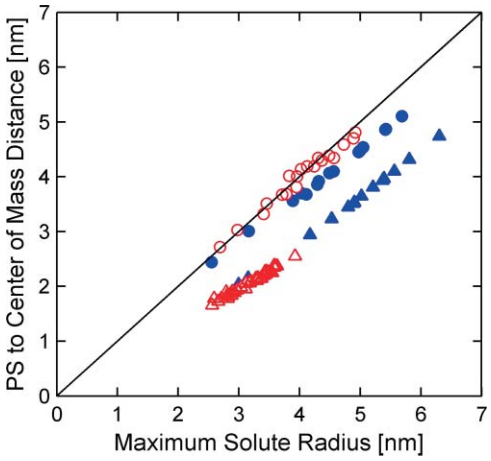

FIG. 7. Mean distance between all PS beads in a nanoparticle and the nanoparticle center of mass vs the maximum solute radius. The statistical uncertainty of each data point is no larger than the symbol size. Symbols are as in Fig. 1. The solid black line of unit slope is a guide to the eye.

nanoparticle surface, whereas the potential used in the DPD simulations is substantially softer, allowing for some minor penetration of the PS beads past the surface. However, for the BD and DPD simulations with the favorable solute–PS interaction, the PS bead penetration into the core is nearly identical.

Figure 8 shows the overall nanoparticle radius versus the number of solute molecules in the core. We have defined the overall radius as the distance between the terminal bead in a PEG block and the center of mass, averaged over all diblocks in the aggregate. In both the BD and DPD simulations, the nanoparticles formed have a larger overall radius when the solute–PS interaction is unfavorable than when it is favorable. This is a result of clustering of the PS beads on the surface, which causes the PEG blocks to pack closer together and elongate more. All of the implicit-solvent nanoparticles appear to have an ∼2 nm larger overall radius than explicit-solvent nanoparticles containing the same number

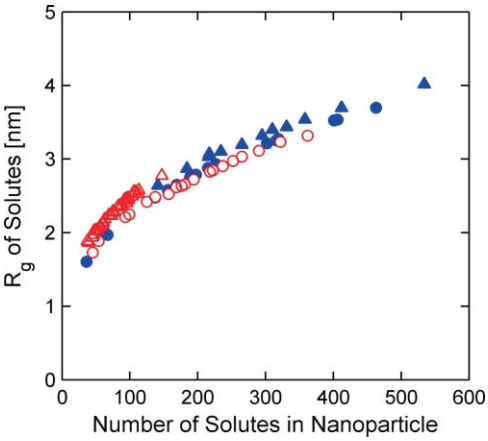

FIG. 6. Radius of gyration of solute beads vs the number of solute molecules in a nanoparticle. The statistical uncertainty of each data point is no larger than the symbol size. Symbols are as in Fig. 1.

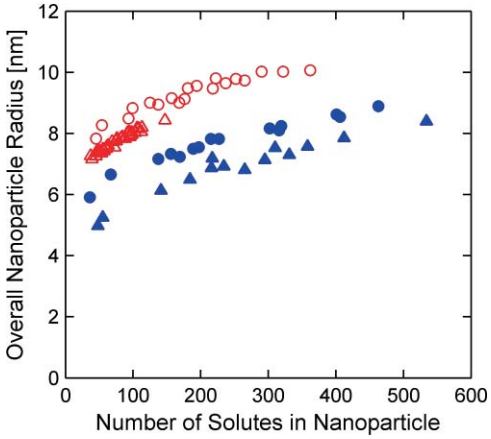

FIG. 8. Overall nanoparticle radius vs number of solutes in the nanoparticle. The overall nanoparticle radius is the distance between the terminal bead in a PEG block and the nanoparticle center of mass, averaged over all diblocks in the nanoparticle. The statistical uncertainty of each data point is no larger than the symbol size. Symbols are as in Fig. 1.

of solute molecules in the core, for both the favorable and unfavorable solute–PS interactions. However, the PEG head-to-tail distance is only about ∼1.2 nm longer for the nanoparticles in the BD simulations as compared to those from the DPD simulations (not shown). This suggests that the PEG blocks in the BD simulations tend to form a larger angle (closer to perpendicular) with the nanoparticle surface than those in the DPD simulations. In a sense, the PEG blocks in the DPD nanoparticles have a greater tendency to "wrap" around the nanoparticle surface than those in the BD simulations. This is likely the result of the Gaussian repulsion potential used in the implicit-solvent model, which causes PEG beads to repel one another, as previously noted.

C. Nanoparticle diffusion coefficients

Experimentally, Kumar *et al*. and others have determined nanoparticle size distributions using dynamic light scattering (DLS).[11–13,16,59] DLS extracts the diffusion coefficient of colloidal particles in a solution and back-calculates their sizes via the Stokes–Einstein relation, rather than directly measuring the particles' sizes. Consequently, we compare the diffusion coefficients of the nanoparticles in our simulations to the values predicted by the Stokes–Einstein relation.

In our simulations, nanoparticle diffusion coefficients were calculated by performing a linear fit of their center-of-mass mean-squared displacements versus time, ignoring the initial ballistic portion of the curve. We used multiple time origins to reduce noise in the data. As with the structural property calculations, data included in the diffusion coefficient calculations were only from the period after the nanoparticle had stopped growing. Figure 9 compares the diffusion coefficients of the nanoparticles formed in the simulations to the values predicted by the Stokes–Einstein relation (solid line). The radius used in Fig. 9 for the nanoparticles is the time average of the distance from the nanoparticle center of mass to the terminal bead in the most extended PEG chain. Clearly, the BD nanoparticles have significantly smaller diffusion coefficients than the values predicted by Stokes–Einstein, more than an order of magnitude in most cases. In contrast, the DPD nanoparticle diffusion coefficients are reasonably close to the Stokes–Einstein relation. In Fig. 10 we plot the BD diffusion coefficients along with the curve $D = kM^{-1}$, where M is the total nanoparticle mass and the constant k has been chosen so that the curve matches the diffusion coefficient of the implicit-solvent model solute. Figure 10 illustrates that clusters of particles in BD follow Rouse behavior ($D \propto M^{-1}$), since there are no hydrodynamic interactions present.[36,60–62] A simple reinterpretation of the time scale would not suffice in producing the proper diffusion coefficients. At any given instant in time, the masses of the aggregates that are present are different, so each aggregate's diffusion coefficient differs from the proper value by a different factor.

The nanoparticles formed in our simulations are quite small compared to those formed in experiments. As the size of the nanoparticles becomes larger, the discrepancy between the diffusion coefficients given by Stokes–Einstein and those observed in BD simulations will grow larger and larger. Consider a nanoparticle with a radius of 50 nm, which will contain ∼620 000 solutes and ∼100 000 diblocks. The Stokes–Einstein relation gives a diffusion coefficient of 4.9 $\times 10^{-8}$ cm^2/s for this nanoparticle. However, if we calculate the mass of such a nanoparticle and plug it into the relationship given by the solid black curve in Fig. 10 (extrapolating the Rouse behavior), we obtain a diffusion coefficient of 6.23 $\times 10^{-12}$ cm^2/s, nearly 10 000 times smaller than the Stokes–Einstein value. Thus, the Rouse scaling inherent in the BD simulations means that one cannot simultaneously capture the correct diffusive behavior of both small structures (single solutes, singles diblocks, or small clusters) and large structures (containing many hundreds or thousands of molecules) without the presence of hydrodynamic interactions. One possible solution to this problem is to employ an algorithm to explicitly add analytical hydrodynamic corrections, but most methods scale very poorly with the number of particles.[63,64]

One might wonder if the BD method itself, rather than the absence of explicit-solvent particles, gives rise

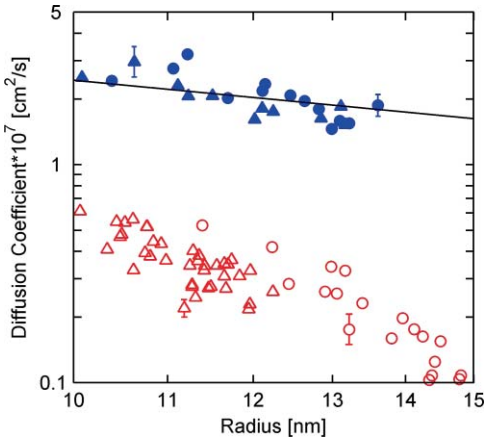

FIG. 9. Diffusion coefficient vs overall nanoparticle radius for the nanoparticles in the BD and DPD simulations. The solid line shows the Stokes–Einstein relation. Error bars show statistical uncertainties for a few representative data points. Symbols are as in Fig. 1.

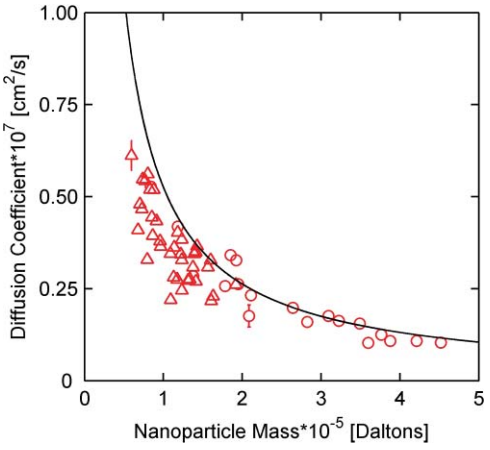

FIG. 10. Diffusion coefficients for nanoparticles from BD simulations, along with the curve $D = kM^{-1}$. The constant k was chosen so that the curve passes through the infinite dilution diffusion coefficient of the solute for the implicit-solvent model. Error bars show statistical uncertainties for a few representative data points. Symbols are as in Fig. 1.

to the incorrect scaling of diffusion coefficients with the implicit-solvent model. One alternative would be to try evolving the implicit-solvent model with the pairwise, momentum-conserving frictional and dissipative forces from the DPD method (this is referred to as the "DPD thermostat"). However, with an implicit-solvent simulation, the result of all forces being between *pairs* of particles and obeying momentum conservation is that an already-formed cluster never sees its center-of-mass momentum changed unless it comes within the interaction range of another cluster. Consequently, the nanoparticle aggregates behave ballistically, rather than diffusively (we confirmed this by running such simulations and plotting the mean-squared displacement versus time for various nanoparticles).

D. Nanoparticle stability

Recently, Budijono *et al.*[16,65] conducted experiments in which they used flash nanoprecipitation to study the surface coverage of PS_{15}-*b*-PEG_{118} on monodisperse 210 nm diameter latex spheres. Although the PS_{15}-*b*-PEG_{118} has a longer PEG block than the diblock used in this work (PS_{10}-*b*-PEG_{68}), these experiments still enable us to put in context the surface area per polymer calculated in our simulations. Budijono *et al.* varied the polymer concentration and determined when free micelles began forming. At this critical concentration, they used DLS and a Baleux assay to determine the average number of diblocks on the surface of each latex sphere, from which they calculated the average surface area covered by each polymer. The area occupied by each polymer was calculated by setting the total area covered by n polymers to the total area available for coverage,

$$n\pi\left(\frac{\xi}{2}\right)^2 = 4\pi\left(\frac{D_{\text{sphere}}}{2}+\frac{\xi}{2}\right)^2, \tag{16}$$

and then solving for the area occupied by a single polymer chain,

$$\pi\left(\frac{\xi}{2}\right)^2 = \frac{\pi}{n}\left(\frac{D_{\text{sphere}}}{1-\frac{2}{\sqrt{n}}}\right)^2. \tag{17}$$

In Eqs. (16) and (17), n represents the number of polymer chains on the surface, D_{sphere} represents the diameter of the core, and ξ represents the "blob size" or diameter of the space that a single polymer occupies on the surface. In their experiments, Budijono *et al.*[16,65] found that the surface area per polymer for PS_{15}-*b*-PEG_{118} was 13.9 nm^2. However, the surface area that the same polymer would occupy if it were in a randomly coiled configuration is 23.8 nm^2.[16]

Figure 11 shows the surface area per diblock for the final nanoparticles formed in the DPD and BD simulations with favorable solute–PS interactions. The diameter used to calculate the surface area per polymer for each nanoparticle was taken as the diameter of a sphere containing the number of solute molecules in that nanoparticle (at the solid density of the solute). For the diblock copolymer used in our simulations, PS_{10}-*b*-PEG_{68}, experimental values of the surface area per polymer are unknown, but the surface area occupied by this polymer in a randomly coiled configuration is

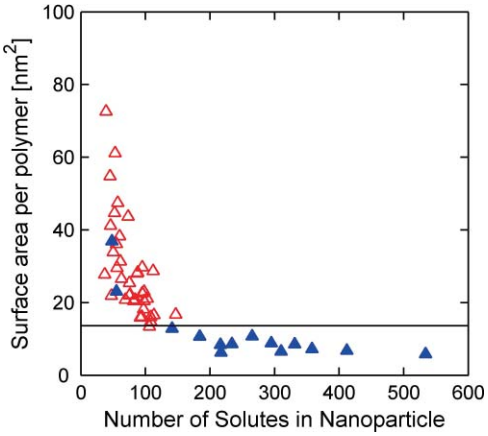

FIG. 11. Surface area per polymer vs number of solutes in nanoparticle for simulations with favorable solute–PS interactions. Symbols are as in Fig. 1. The solid line represents the surface area occupied by a randomly coiled diblock (Ref. 16).

13.6 nm^2.[16] Based upon the experiments of Budijono *et al.* using a similar polymer,[16,65] we would expect the surface area per polymer on the nanoparticle surface to be roughly half of the value calculated for the random coil configuration. The largest particles formed in the DPD simulations have an area per polymer that is roughly half of the value for the isolated, randomly coiled polymer. On the other hand, the BD particles are stable and resist fusion even when the surface area per polymer is two to four times greater than the surface area occupied by polymers in DPD nanoparticles. For the DPD data points shown, the three smallest nanoparticles have a large surface area per polymer. Each of these nanoparticles was the smallest and most poorly covered in its simulation box (data shown are from three separate simulations), but all other nanoparticles were sufficiently well covered to prevent any further fusion from occurring.

In order to gain more insight as to why the BD nanoparticles stop fusing earlier than similar DPD nanoparticles of the same size and surface coverage, we ran controlled simulations in which we placed two identical nanoparticles in a simulation box and monitored the distance between the nanoparticle centers of mass. The nanoparticles we used contained 100 solutes and 16 polymers each (roughly the size at which the BD nanoparticles stopped fusing, with a surface area per polymer of ~40 nm^3) and utilized the favorable solute–PS interactions. The DPD nanoparticles rapidly fused together, whereas the BD nanoparticles "collided" many times, but could not get close enough to fuse. This suggests that the DPD nanoparticles require substantially more polymers per unit surface area than the BD nanoparticles before they become stable with respect to fusion with one another, as illustrated in Fig. 11.

E. Relative efficiency of BD versus DPD

Both the BD and DPD simulations utilized a 50 × 50 × 50 nm system size, but the BD simulations used 3995 total particles versus 375 000 for the DPD simulations (both simulations contained the same number of diblock and solute

molecules). A single BD simulation of 60 μs of effective real time took 7.5 h on a single core of a 2.77 GHz Intel Core 2 Duo processor, whereas a single DPD simulation of the same effective time running on 16 of the same cores in parallel took about 207 h. The 7.5 CPU-h required for a BD simulation was ~440 times less than the ~3300 CPU-h required for a DPD simulation of the same system size and simulation length.

It appears at first that BD simulations are much more efficient than the DPD simulations and may provide a means for simulating larger systems for longer times. However, as previously mentioned, the nanoparticle diffusion coefficients in the BD simulations are substantially smaller than those given by the Stokes–Einstein relation. For a particle with an overall radius of 10 nm, the BD diffusion coefficient is roughly 20–30 times less than the Stokes–Einstein value, and for a radius of 50 nm the diffusion coefficient is nearly 10 000 times smaller. If one were to simulate the flash nanoprecipitation process and incorporate the effects of mixing in the solvent, the result would be that the particles would grow larger than the ~10 nm radius particles observed in our simulations. As the particles grew larger, the BD simulations would *effectively* become slower, because the nanoparticle diffusion coefficients (and, thus, the number of collisions that can lead to nanoparticle fusion events) would drastically stray away from Stokes–Einstein, as illustrated above. Based upon the scaling of diffusion coefficients seen in our simulations, the increase in computational efficiency of the BD simulations (a factor of ~440) would be canceled out when the overall nanoparticle radii reached ~17 nm.

IV. CONCLUSIONS

In summary, we have developed an explicit-solvent DPD model and an implicit-solvent BD model to study the flash nanoprecipitation process in the limit of instantaneous mixing of solvent with antisolvent. Both models were parameterized based on the recent experiments of Kumar *et al.*[13] The structural properties of the nanoparticles formed in both sets of simulations are very similar; however, the PEG chains in the stabilizing layer around the nanoparticles are more extended in the BD simulations compared to the DPD simulations. The DPD nanoparticles are stable when the surface area per polymer is approximately half of that of a chain in an isolated random coil configuration, whereas the BD nanoparticles are stable when the surface area per polymer is two to four times larger. The repulsion between PEG chains in the BD simulations produces artificially stable nanoparticles, with regard to fusion between them. The PEG chains in the implicit-solvent model form a repulsive "cloud" around the outside of the particle, whereas those in the explicit-solvent tend to behave in a more stringlike fashion. Implementing a less coarse-grained model for the PEG chain in the BD simulations (i.e., using more than eight beads to represent the 68 monomers in the PEG_{3000} chain) and a shorter-ranged potential (i.e., a truncated Weeks–Chandler–Andersen (WCA) potential) between beads may be a way of eliminating this artifact.

The implicit-solvent nanoparticles grow at a significantly slower rate than the explicit-solvent ones, which is largely a result of the discrepancy in their diffusion coefficients. We have shown that the diffusion coefficients of the DPD particles are near the theoretical values predicted by the Stokes–Einstein relationship ($D \propto R^{-1}$), whereas the diffusion coefficients of the BD nanoparticles obey Rouse scaling ($D \propto M^{-1}$). As the particles become larger, the BD diffusion coefficients become progressively smaller with respect to those given by the Stokes–Einstein relationship. This effectively slows down the BD simulations, and at some point they become effectively slower than the explicit-solvent DPD simulations, despite being ~440 times more computationally efficient (on the basis of CPU time needed for a typical system).

Our simulations produced particles that were quite small compared to those created in flash nanoprecipitation experiments. One primary reason for this is that we investigated the limit of infinitely fast mixing of solvent and antisolvent. In reality, the mixing process is complex, with the solvent and antisolvent mixture becoming homogeneous on successively smaller length scales as time progresses. Since the solute molecules are present at a higher supersaturation ratio than the diblock copolymers, they begin to precipitate before the copolymers arrive at the nanoparticle surfaces to arrest their growth and stabilize them—this suggests that longer mixing times will produce larger particles. In order to simulate the formation of larger particles than those formed in this work, larger systems and longer simulations times are needed. An implicit-solvent approach without hydrodynamic interactions may seem like a computationally efficient way to achieve this feat at first, but we have demonstrated some pitfalls associated with this approach, mainly that the aggregated structures have drastically incorrect diffusive behavior. On the other hand, the DPD method produces more realistic results, but the explicit representation of the solvent limits the size of the systems that can be investigated. Nonequilibrium simulations of highly dilute systems in which hydrodynamics are important will continue to present a significant challenge to researchers.

ACKNOWLEDGMENTS

Financial support for this work was provided by a NIRT award from the National Science Foundation (NSF) (CBET-0506966), with additional support from the Princeton Center for Complex Materials, a National Science Foundation (NSF) MRSEC (Award DMR-0819860), from National Science Foundation (NSF) grant (CMMI-1002469), and from the US DOE (DE-SC 0002097). Additionally, the authors are grateful for discussions with Professor Robert K. Prud'homme, Varun Kumar, Stephanie J. Budijono, and Suzanne M. D'Addio.

[1] C. A. Lipinski, J. Pharmacol. Toxicol. Methods **44**, 235 (2000).
[2] R. Gref, Y. Minamitake, M. T. Peracchia, V. Trubetskoy, V. Torchilin, and R. Langer, Science **263**, 1600 (1994).
[3] K. S. Soppimath, T. M. Aminabhavi, A. R. Kulkarni, and W. E. Rudzinski, J. Controlled Release **70**, 1 (2001).
[4] M. L. Adams, A. Lavasanifar, and G. S. Kwon, J. Pharm. Sci. **92**, 1343 (2003).
[5] B. K. Johnson and R. K. Prud'homme, Aust. J. Chem. **56**, 1021 (2003).
[6] H. F. Liang, C. T. Chen, S. C. Chen, A. R. Kulkarni, Y. L. Chiu, M. C. Chen, and H. W. Sung, Biomaterials **27**, 2051 (2006).
[7] N. G. Portney and M. Ozkan, Anal. Bioanal. Chem. **384**, 620 (2006).
[8] M. E. Napier and J. M. Desimone, Polym. Rev. **47**, 321 (2007).
[9] J. Shan and H. Tenhu, Chem. Commun. (Cambridge) **44**, 4580 (2007).

[10]M. Akbulut, P. Ginart, M. E. Gindy, C. Theriault, K. H. Chin, W. Soboyejo, and R. K. Prud'homme, Adv. Funct. Mater. **19**, 718 (2009).
[11]M. E. Gindy, A. Z. Panagiotopoulos, and R. K. Prud'homme, Langmuir **24**, 83 (2008).
[12]T. Chen, S. M. D'Addio, M. T. Kennedy, A. Swietlow, I. G. Kevrekidis, A. Z. Panagiotopoulos, and R. K. Prud'homme, Nano Lett. **9**, 2218 (2009).
[13]V. Kumar, L. Wang, M. Riebe, H. H. Tung, and R. K. Prud'homme, Mol. Pharmacol. **6**, 1118 (2009).
[14]V. Kumar and R. K. Prud'homme, J. Pharm. Sci. **97**, 4904 (2008).
[15]V. Kumar, S. Y. Hong, A. E. Maciag, J. E. Saavedra, D. H. Adamson, R. K. Prud'homme, L. K. Keefer, and H. Chakrapani, Mol. Pharmacol. **7**, 291 (2010).
[16]S. J. Budijono, B. Russ, W. Saad, D. H. Adamson, and R. K. Prud'homme, Colloids Surf. A **360**, 105 (2010).
[17]S. Y. Kim and Y. M. Lee, Biomaterials **22**, 1697 (2001).
[18]S. Mornet, S. Vasseur, F. Grasset, and E. Duguet, J. Mater. Chem. **14**, 2161 (2004).
[19]M. E. Akerman, W. C. W. Chan, P. Laakkonen, S. N. Bhatia, and E. Ruoslahti, Proc. Natl. Acad. Sci. USA **99**, 12617 (2002).
[20]J. K. Zhou, C. Leuschner, C. Kumar, J. F. Hormes, and W. O. Soboyejo, Biomaterials **27**, 2001 (2006).
[21]Y. Zhang, N. Kohler, and M. Q. Zhang, Biomaterials **23**, 1553 (2002).
[22]S. Sengupta, D. Eavarone, I. Capila, G. L. Zhao, N. Watson, T. Kiziltepe, and R. Sasisekharan, Nature (London) **436**, 568 (2005).
[23]G. Kong, R. D. Braun, and M. W. Dewhirst, Cancer Res. **60**, 4440 (2000).
[24]B. Russ, Y. Liu, and R. K. Prud'homme, Chem. Eng. Commun. **197**, 1068 (2010).
[25]Y. Liu, C. Y. Cheng, R. K. Prud'homme, and R. O. Fox, Chem. Eng. Sci. **63**, 2829 (2008).
[26]M. Laradji and M. J. A. Hore, J. Chem. Phys. **121**, 10641 (2004).
[27]F. A. Detcheverry, H. M. Kang, K. C. Daoulas, M. Muller, P. F. Nealey, and J. J. de Pablo, Macromolecules **41**, 4989 (2008).
[28]V. Kalra, S. Mendez, F. Escobedo, and Y. L. Joo, J. Chem. Phys. **128**, 164909 (2008).
[29]Q. H. Zeng, A. B. Yu, and G. Q. Lu, Prog. Polym. Sci. **33**, 191 (2008).
[30]H. Y. Chen and E. Ruckenstein, J. Chem. Phys. **131**, 244904 (2009).
[31]V. Kalra and Y. L. Joo, J. Chem. Phys. **131**, 214904 (2009).
[32]J. H. Huang and Y. M. Wang, J. Phys. Chem. B **111**, 7735 (2007).
[33]S. Chen, C. Guo, G. H. Hu, H. Z. Liu, X. F. Liang, J. Wang, J. H. Ma, and L. Zheng, Colloid Polym. Sci. **285**, 1543 (2007).
[34]L. Zhang, J. Lin, and S. Lin, Macromolecules **40**, 5582 (2007).
[35]J. Huang, M. Luo, and Y. Wang, J. Phys. Chem. B **112**, 6735 (2008).
[36]T. Chen, A. P. Hynninen, R. K. Prud'homme, I. G. Kevrekidis, and A. Z. Panagiotopoulos, J. Phys. Chem. B **112**, 16357 (2008).
[37]R. Agrawal and D. A. Kofke, Mol. Phys. **85**, 43 (1995).
[38]S. Plimpton, J. Comput. Phys. **117**, 1 (1995).
[39]P. J. Hoogerbrugge and J. Koelman, Europhys. Lett. **19**, 155 (1992).
[40]R. D. Groot and P. B. Warren, J. Chem. Phys. **107**, 4423 (1997).
[41]P. Espanol and P. Warren, Europhys. Lett. **30**, 191 (1995).
[42]S. Kawaguchi, G. Imai, J. Suzuki, A. Miyahara, and T. Kitano, Polymer **38**, 2885 (1997).
[43]K. Mortensen, W. Brown, K. Almdal, E. Alami, and A. Jada, Langmuir **13**, 3635 (1997).
[44]Y. J. Sheng, T. Y. Wang, W. M. Chen, and H. K. Tsao, J. Phys. Chem. B **111**, 10938 (2007).
[45]M. A. Floriano, E. Caponetti, and A. Z. Panagiotopoulos, Langmuir **15**, 3143 (1999).
[46]K. Meguro, Y. Takasawa, N. Kawahashi, Y. Tabata, and M. Ueno, J. Colloid Interface Sci. **83**, 50 (1981).
[47]L. M. Bronstein, D. M. Chernyshov, G. I. Timofeeva, L. V. Dubrovina, P. M. Valetsky, and A. R. Khokhlov, Langmuir **15**, 6195 (1999).
[48]J. R. Spaeth, T. Dale, I. G. Kevrekidis, and A. Z. Panagiotopoulos, Ind. Eng. Chem. Res. **50**, 69 (2010).
[49]C. M. Wijmans, B. Smit, and R. D. Groot, J. Chem. Phys. **114**, 7644 (2001).
[50]W. Jiang, J. Huang, Y. Wang, and M. Laradji, J. Chem. Phys. **126**, 044901 (2007).
[51]R. D. Groot, J. Chem. Phys. **118**, 11265 (2003).
[52]I. V. Pivkin and G. E. Karniadakis, J. Chem. Phys. **124**, 184101 (2006).
[53]R. D. Groot, Langmuir **16**, 7493 (2000).
[54]R. D. Groot and K. L. Rabone, Biophys. J. **81**, 725 (2001).
[55]R. M. Fuchslin, H. Fellermann, A. Eriksson, and H.-J. Ziock, J. Chem. Phys. **130**, 214102 (2009).
[56]S. J. Marrink, D. P. Tieleman, and A. E. Mark, J. Phys. Chem. B **104**, 12165 (2000).
[57]D. Evans and H. Wennerstrom, *The Colloidal Domain: Where Physics, Chemistry, Biology, and Technology Meet* (Wiley, New York, 1999).
[58]See supplementary material at http://dx.doi.org/10.1063/1.3580293 for movie files associated with Figs. 4 and 5.
[59]Z. X. Zhu, J. L. Anacker, S. X. Ji, T. R. Hoye, C. W. Macosko, and R. K. Prud'homme, Langmuir **23**, 10499 (2007).
[60]L. Isella and Y. Drossinos, Phys. Rev. E **82**, 011404 (2010).
[61]P. E. Rouse, J. Chem. Phys. **21**, 1272 (1953).
[62]T. T. Pham, U. D. Schiller, J. R. Prakash, and B. Dunweg, J. Chem. Phys. **131**, 164114 (2009).
[63]D. L. Ermak and J. A. McCammon, J. Chem. Phys. **69**, 1352 (1978).
[64]T. Geyer and U. Winter, J. Chem. Phys. **130**, 8 (2009).
[65]S. J. Budijono and R. K. Prud'homme, personal communication (December 16, 2010).